

Graph-based Transforms for Video Coding

Hilmi E. Egilmez, *Member, IEEE*, Yung-Hsuan Chao, *Member, IEEE* and Antonio Ortega, *Fellow, IEEE*

Abstract—In many state-of-the-art compression systems, signal transformation is an integral part of the encoding and decoding process, where transforms provide compact representations for the signals of interest. This paper introduces a class of transforms called graph-based transforms (GBTs) for video compression, and proposes two different techniques to design GBTs. In the first technique, we formulate an optimization problem to learn graphs from data and provide solutions for optimal separable and nonseparable GBT designs, called GL-GBTs. The optimality of the proposed GL-GBTs is also theoretically analyzed based on Gaussian-Markov random field (GMRF) models for intra and inter predicted block signals. The second technique develops edge-adaptive GBTs (EA-GBTs) in order to flexibly adapt transforms to block signals with image edges (discontinuities). The advantages of EA-GBTs are both theoretically and empirically demonstrated. Our experimental results show that the proposed transforms can significantly outperform the traditional Karhunen-Loeve transform (KLT).

Index Terms—Transform coding, predictive coding, graph-based transforms, video coding, compression, optimization, statistical modeling.

I. INTRODUCTION

Predictive transform coding is a fundamental compression technique adopted in many block-based image and video compression systems, where block signals are initially predicted from a set of available (already coded) reference pixels, and then the resulting residual block signals are transformed (generally by a linear transformation) to decorrelate residual pixel values for effective compression. After prediction and transformation steps, a typical image/video compression system applies quantization and entropy coding to convert transform coefficients into a stream of bits. Fig. 1 illustrates a representative encoder-decoder architecture comprising three basic components, (i) prediction, (ii) transformation, (iii) quantization and entropy coding, which are implemented in state-of-the-art compression standards such as JPEG [5], HEVC [6], VP9 [7], AV1 [8] and VVC [9]. This paper focuses mainly on the transformation component of video coding and develops techniques to design orthogonal transforms, called graph-based transforms (GBTs), adapting diverse characteristics of video signals.

In predictive transform coding of video, the prediction is generally carried out by choosing one among multiple intra and inter prediction modes in order to exploit spatial and temporal redundancies between block signals. On the other

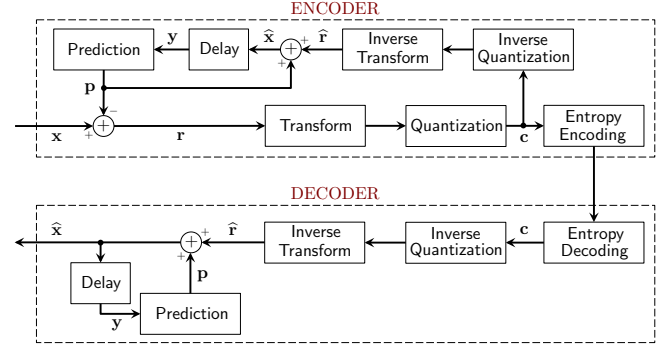


Fig. 1. Building blocks of a typical video encoder and decoder consisting of three main steps, which are (i) prediction, (ii) transformation, (iii) quantization and entropy coding.

hand, for the transformation, typically a single transform such as the discrete cosine transform (DCT-2) is applied in a separable manner to rows and columns of each residual block. The main problem of using fixed block transforms is the implicit assumption that all residual blocks share the same statistical properties. However, residual blocks can have very diverse statistical characteristics depending on the video content and the prediction mode (as will be demonstrated by some of the experiments in Section VII). The HEVC [6] standard, partially addresses this problem by allowing the use of the asymmetric discrete sine transform (ADST or DST-7) in addition to the DCT-2 for small (i.e., 4×4) intra predicted blocks [10]. Yet, it has been shown that better compression can be achieved by using data-driven transform designs that adapt to statistical properties of residual blocks [11]–[20].

The majority of prior studies about transforms for video coding focus on developing transforms for intra predicted residuals. In [11], a mode-dependent transform (MDT) scheme is proposed by designing a Karhunen-Loeve transform (KLT) for each intra prediction mode. In [12], [13], the MDT scheme is similarly implemented for the HEVC standard, where a single KLT is trained for each intra prediction mode offered in HEVC. Moreover in [15]–[18], [21], the authors demonstrate considerable coding gains over the MDT method by using the rate-distortion optimized transformation (RDOT) scheme, which suggests designing multiple transforms for each prediction mode so that the encoder can select a transform (from the predetermined set of transforms) by minimizing a rate-distortion (RD) cost. More recently, the VVC standard [9] has adopted simplified variants of the RDOT-based methods in [15], [21]. Since the RDOT scheme allows the flexibility of selecting a transform on a per-block basis at the encoder side, it provides better adaptation to residual blocks with different statistical characteristics as compared to the MDT scheme. However, all of these methods rely on KLTs derived from sample covariance matrices, which may not be good estimators

H.E. Egilmez and Y.-H. Chao are with Qualcomm Technologies Inc., San Diego, CA, 92121 USA. A. Ortega is with the Department of Electrical Computer Engineering, University of Southern California, Los Angeles, CA, 90084 USA. Contact author e-mail: hegilmez@qti.qualcomm.com.

This work has been done while H.E. Egilmez and Y.-H. Chao were with University of Southern California. Earlier versions of the work were presented at the IEEE International Conference on Image Processing in [1], [2] and in the PhD dissertations [3], [4].

for the true covariances of models, especially when the number of data samples is small [22], [23]. Indeed, it has been shown that more accurate model estimates can be obtained using inverse covariance estimation methods [23], [24] or graph learning methods, such as those introduced in our prior work [25], [26].

This paper proposes a novel graph-based modeling framework to design GBTs, where the models of interest are based on Gaussian-Markov random fields (GMRFs) whose inverse covariances are graph Laplacian matrices. The proposed framework consists of two distinct techniques to develop GBTs for video coding, called GL-GBTs and EA-GBTs:

- *Graph learning for GBT (GL-GBT) design:* A graph learning problem with a maximum-likelihood (ML) criterion is formulated and solved to estimate a graph Laplacian matrix from training data. In order to construct separable and nonseparable GBTs, two instances of the proposed problem with different connectivity constraints are solved by applying the graph learning algorithm introduced in our prior work [25]. Then, the GBTs are constructed by the eigendecomposition of the graph Laplacians of the learned graphs. As the KLT, a GL-GBT is learned from a sample covariance, but in addition, it incorporates Laplacian and structural constraints reflecting the inherent model assumptions about the video signal. From a statistical learning perspective, the main advantage of the proposed GL-GBT over the KLT is that the GL-GBT requires learning fewer model parameters from training data, and thus can lead to a more robust transform allowing better compression for the block signals outside of the training dataset. GL-GBTs can be adopted to improve existing MDT or RDOT schemes using KLTs.
- *Edge-adaptive GBT (EA-GBT) design:* To adapt transforms for block signals with image edges¹, we develop edge-adaptive GBTs (EA-GBTs) which are designed on a per-block basis. These lead to a block-adaptive transform scheme, where transforms are derived from graph Laplacians whose weights are modified based on image edges detected in a residual block.

In the literature, there are a few studies on model-based transform designs for image and video coding. In [27], [28], the authors present a graph-based probabilistic framework for predictive video coding and use that to justify the optimality of DCT, yet optimal graph/transform design is out of their scope. In our previous work [29], we present a comparison of various instances of different graph learning problems for nonseparable image modeling. The present paper theoretically and empirically validates one of the conclusions in [29], which suggests the use of GBTs derived from graph Laplacian matrices for image compression. In [30], a block-adaptive scheme is proposed for image compression with GBTs, where a graph is constructed for each block signal by minimizing a regularized Laplacian quadratic term used as the proxy for actual RD cost. On the other hand, in our present work, graphs are estimated from aggregate data statistics or constructed using image edge

information. Then, the encoder selects the best transform based on exact RD measures. Moreover, Shen *et al.* [31] propose edge adaptive transforms (EAT) specifically for depth-map compression, and Hu *et al.* [32] extend EATs for piecewise-smooth image compression. Although our proposed EA-GBTs adopt some basic concepts originally introduced in [31], our graph construction method is different (in terms of image edge detection) and provides better compression for residual signals.

The main contributions of this paper can be summarized as follows:

- We propose graph learning techniques for separable and nonseparable GBTs (i.e., GBSTs and GBNTs, respectively) and present a theoretical justification of their use for coding residual block signals modeled using GMRFs.
- As an extension of the 1-D GMRF models used to design GBSTs for intra and inter predicted signals in our previous work [2], we present a general 2-D GMRF model for GBNTs and analyze its optimality.
- We apply EA-GBTs to intra and inter predicted blocks, while our prior work in [1] focused only on inter predicted blocks. In addition to the experimental results, we further derive some theoretical results and discuss the cases in which EA-GBTs are useful.
- We present comprehensive experimental results comparing the compression performances obtained using KLTs, GL-GBTs and EA-GBTs.

The rest of the paper is organized as follows. Section II presents the basic notation and definitions used throughout the paper. Section III introduces 2-D GMRFs used for modeling the video signals and discusses graph-based interpretations. In Section IV, the GBT design problem is formulated as a graph Laplacian estimation problem, and solutions for optimal GBT construction are proposed. Section V presents EA-GBTs. Graph-based interpretations of residual block signal characteristics are discussed in Section VI by empirically validating the theoretical observations. Experimental results are presented in Section VII, and Section VIII draws concluding remarks.

II. NOTATION AND PRELIMINARIES

Throughout the paper, lowercase normal (e.g., a and θ), lowercase bold (e.g., \mathbf{a} and $\boldsymbol{\theta}$) and uppercase bold (e.g., \mathbf{A} and $\boldsymbol{\Theta}$) letters denote scalars, vectors and matrices, respectively. Unless otherwise stated, calligraphic capital letters (e.g., \mathcal{E} and \mathcal{S}) represent sets. Notation is summarized in Table I.

In this paper, we focus on connected, undirected, weighted simple graphs with nonnegative edge weights [33]. We next present basic definitions related to graphs.

Definition 1 (Weighted Graph). The graph $\mathcal{G}=(\mathcal{V}, \mathcal{E}, f_w, f_v)$ is a weighted graph with n vertices in the set $\mathcal{V}=\{v_1, \dots, v_n\}$. The edge set $\mathcal{E}=\{e \mid f_w(e) \neq 0, \forall e \in \mathcal{P}_u\}$ is a subset of \mathcal{P}_u , the set of all unordered pairs of vertices, where $f_w((v_i, v_j)) \geq 0$ for $i \neq j$ is a real-valued edge weight function, and $f_v(v_i)$ for $i=1, \dots, n$ is a real-valued vertex (self-loop) weight function.

Definition 2 (Algebraic representations of graphs). For a given weighted graph $\mathcal{G}=(\mathcal{V}, \mathcal{E}, f_w)$ with n vertices, v_1, \dots, v_n :

¹We use the term *image edge* to distinguish edges in image/video signals with edges in graphs.

TABLE I
LIST OF SYMBOLS AND THEIR MEANING

Symbols	Meaning
$\mathcal{G} \mid \mathbf{L}$	weighted graph graph Laplacian matrix
$n \mid N$	number of vertices block size ($N \times N$)
$\mathbf{I} \mid \mathbf{1}$	identity matrix vector of all ones
$\Theta^\top \mid \theta^\top$	transpose of Θ transpose of θ
$(\Theta)_{ij}$	entry of Θ at i -th row and j -th column
$(\theta)_i$	i -th entry of θ
$(\theta)_\mathcal{S}$	subvector of θ formed by selecting indexes in \mathcal{S}
$\geq (\leq)$	element-wise greater (less) than or equal to operator
$\Theta \succeq 0$	Θ is a positive semidefinite matrix
$\Theta^{-1} \mid \det(\Theta)$	inverse of Θ determinant of Θ
$\text{Tr} \mid \log\det(\Theta)$	trace operator natural logarithm of $\det(\Theta)$
$\text{diag}(\theta)$	diagonal matrix formed by elements of θ
$\text{ddiag}(\Theta)$	diagonal matrix formed by diagonal elements of Θ
$\mathbf{x} \sim \mathcal{N}(\mathbf{0}, \Sigma)$	zero-mean multivariate Gaussian with covariance Σ

The *adjacency matrix* of \mathcal{G} is an $n \times n$ symmetric matrix, \mathbf{W} , such that $(\mathbf{W})_{ij} = (\mathbf{W})_{ji} = f_w((v_i, v_j))$ for $(v_i, v_j) \in \mathcal{P}_u$. The *degree matrix* of \mathcal{G} is an $n \times n$ diagonal matrix, \mathbf{D} , with entries $(\mathbf{D})_{ii} = \sum_{j=1}^n (\mathbf{W})_{ij}$ and $(\mathbf{D})_{ij} = 0$ for $i \neq j$. The *self-loop matrix* of \mathcal{G} is an $n \times n$ diagonal matrix, \mathbf{V} , with entries $(\mathbf{V})_{ii} = f_v(v_i)$ for $i = 1, \dots, n$ and $(\mathbf{V})_{ij} = 0$ for $i \neq j$. If \mathcal{G} is a simple weighted graph, then $\mathbf{V} = \mathbf{0}$.

The *connectivity matrix* of \mathcal{G} is an $n \times n$ matrix, \mathbf{A} , such that $(\mathbf{A})_{ij} = 1$ if $(\mathbf{W})_{ij} \neq 0$, and $(\mathbf{A})_{ij} = 0$ if $(\mathbf{W})_{ij} = 0$ for $i, j = 1, \dots, n$, where \mathbf{W} is the adjacency matrix of \mathcal{G} .

The *combinatorial graph Laplacian (CGL)* of graph \mathcal{G} is defined as $\mathbf{L} = \mathbf{D} - \mathbf{W}$.

The *generalized graph Laplacian (GGL)* of graph \mathcal{G} is defined as $\mathbf{L} = \mathbf{D} - \mathbf{W} + \mathbf{V}$, which reduces to the combinatorial graph Laplacian when there are no self-loops ($\mathbf{V} = \mathbf{0}$).

Definition 3 (Graph-based Transform (GBT)). Let \mathbf{L} be a graph Laplacian of a graph \mathcal{G} . The graph-based transform is the orthogonal matrix \mathbf{U} , satisfying $\mathbf{U}^\top \mathbf{U} = \mathbf{I}$, obtained by eigendecomposition of $\mathbf{L} = \mathbf{U} \mathbf{\Lambda} \mathbf{U}^\top$, where $\mathbf{\Lambda}$ is the diagonal matrix consisting of eigenvalues of \mathbf{L} (graph frequencies).

As formally stated in the following proposition, GBTs are invariant under (i) constant scaling of graph weights and (ii) addition of a constant self-loop weight to all vertices.

Proposition 1. Let \mathbf{U} be a GBT diagonalizing graph Laplacian \mathbf{L} . The same \mathbf{U} also diagonalizes Laplacians of the form $\tilde{\mathbf{L}} = c_1 \mathbf{L} + c_2 \mathbf{I}$, where c_1 and c_2 are real-valued scalars.

Proof. The proof is straightforward from Definition 3. \square

III. GRAPH-BASED MODELS AND TRANSFORMS FOR VIDEO BLOCK SIGNALS

For modeling video block signals, we use Gaussian Markov random fields (GMRFs), which provide a probabilistic interpretation for our graph-based framework. Assuming that the random vector of interest $\mathbf{x} \in \mathbb{R}^n$ has zero mean², a GMRF

²The zero mean assumption is made to simplify the notation. The models can be trivially extended to GMRFs with nonzero mean.

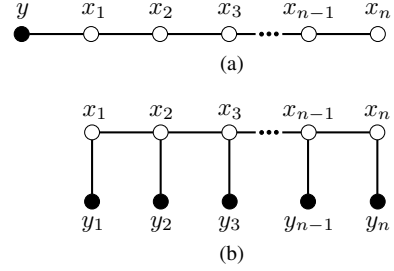


Fig. 2. 1-D GMRF models for (a) intra and (b) inter predicted signals. Black filled vertices represent the reference pixels and unfilled vertices denote pixels to be predicted and then transform coded.

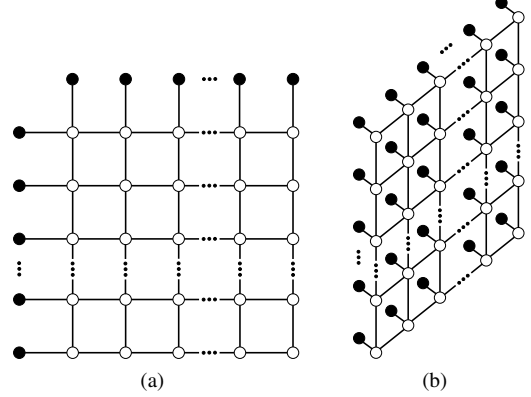


Fig. 3. 2-D GMRF models for (a) intra and (b) inter predicted signals. Black filled vertices correspond to reference pixels obtained (a) from neighboring blocks and (b) from other frames via motion compensation. Unfilled vertices denote the pixels to be predicted and then transform coded.

model for \mathbf{x} is defined based on a precision matrix $\mathbf{\Omega}$, so that \mathbf{x} has a multivariate Gaussian distribution, $\mathbf{x} \sim \mathcal{N}(\mathbf{0}, \mathbf{\Omega}^{-1})$,

$$p(\mathbf{x}|\mathbf{\Omega}) = \frac{1}{(2\pi)^{n/2} \det(\mathbf{\Omega})^{-1/2}} \exp\left(-\frac{1}{2} \mathbf{x}^\top \mathbf{\Omega} \mathbf{x}\right). \quad (1)$$

with covariance matrix $\mathbf{\Sigma} = \mathbf{\Omega}^{-1}$. The entries of the precision matrix $\mathbf{\Omega}$ can be interpreted in terms of conditional dependence relations among variables,

$$\mathbb{E}[x_i | (\mathbf{x})_{\mathcal{S} \setminus \{i\}}] = -\frac{1}{(\mathbf{\Omega})_{ii}} \sum_{j \in \mathcal{S} \setminus \{i\}} (\mathbf{\Omega})_{ij} x_j \quad (2)$$

$$\text{Prec}[x_i | (\mathbf{x})_{\mathcal{S} \setminus \{i\}}] = (\mathbf{\Omega})_{ii} \quad (3)$$

$$\text{Corr}[x_i x_j | (\mathbf{x})_{\mathcal{S} \setminus \{i, j\}}] = -\frac{(\mathbf{\Omega})_{ij}}{\sqrt{(\mathbf{\Omega})_{ii} (\mathbf{\Omega})_{jj}}} \quad i \neq j, \quad (4)$$

where $\mathcal{S} = \{1, \dots, n\}$ is the index set for $\mathbf{x} = [x_1, \dots, x_n]^\top$. The conditional expectation in (2) gives the best minimum mean square error (MMSE) estimate of x_i using all other random variables. The relation in (3) corresponds to the *precision* of x_i and (4) to the *partial correlation* between x_i and x_j (i.e., correlation between random variables x_i and x_j given all other variables in \mathbf{x}). For example, if x_i and x_j are conditionally independent (i.e., $(\mathbf{\Omega})_{ij} = 0$), there is no edge between corresponding vertices v_i and v_j . If all partial correlations are nonnegative (i.e., off-diagonal elements of $\mathbf{\Omega}$ are nonpositive), then the model in (1) is classified as *attractive GMRF* [25], [34], [35], whose precision matrix satisfies the following proposition [2], [25].

Proposition 2. A GMRF model is attractive if and only if its precision matrix $\mathbf{\Omega}$ is a generalized graph Laplacian matrix.

Proof. The proof is straightforward by the definitions. \square

In statistical modeling of image/video signals, it is generally assumed that adjacent pixel values are positively correlated [36], [37]. The assumption is intuitively reasonable for video signals, since neighboring pixel values are often similar to each other due to spatial and temporal redundancy. With this general assumption, we propose attractive GMRFs to model intra/inter predicted video block signals. Figs. 2 and 3 illustrate the 1-D and 2-D GMRFs defining *line* and *grid* graphs that are used to design separable and nonseparable GBTs, respectively.

We formally define GBST and GBNT as follows.

Definition 4 (Graph-based Separable Transform–GBST). Let \mathbf{U}_{row} and \mathbf{U}_{col} be $N \times N$ GBTs associated with two line graphs with N vertices, then the GBST of an $N \times N$ matrix \mathbf{X} is

$$\hat{\mathbf{X}} = \mathbf{U}_{\text{col}}^T \mathbf{X} \mathbf{U}_{\text{row}}, \quad (5)$$

where \mathbf{U}_{row} and \mathbf{U}_{col} are the transforms applied to rows and columns of the block signal \mathbf{X} , respectively.

Definition 5 (Graph-based Nonseparable Transform–GBNT). Let \mathbf{U} be an $N^2 \times N^2$ GBT associated with a graph with N^2 vertices, then the GBNT of an $N \times N$ matrix \mathbf{X} is

$$\hat{\mathbf{X}} = \text{block}(\mathbf{U}^T \text{vec}(\mathbf{X})), \quad (6)$$

where \mathbf{U} is applied on vectorized signal $\mathbf{x} = \text{vec}(\mathbf{X})$, and the block operator restructures the signal back in block form.

In our previous work [2], we introduced the 1-D GMRFs illustrated in Fig. 2 for intra/inter predicted signals and also derived closed-form expressions of their precision matrices (i.e., Ω). The following section presents a unified 2-D extension of those models. While the work in [28] has noted the relation between graph Laplacians and GMRFs in the context of predictive transform coding, the following section further shows that residual signals obtained from MMSE prediction follow an attractive GMRF model. Hence, the optimal linear transform decorrelating such residual signals is a GBT derived from a GGL.

A. 2-D GMRF Model for Residual Signals

We introduce a general 2-D GMRF model for intra/inter predicted $N \times N$ block signals depicted in Fig. 3 by deriving the precision matrix of the residual signal \mathbf{r} , obtained after predicting the signal $\mathbf{x} = [x_1 \ x_2 \ \cdots \ x_n]^T$ with $n = N^2$ from n_p reference samples in $\mathbf{y} = [y_1 \ y_2 \ \cdots \ y_{n_p}]^T$ (i.e., predicting unfilled vertices from black filled vertices in Fig. 3), where \mathbf{x} and \mathbf{y} are zero-mean and jointly Gaussian with respect to the following attractive 2-D GMRF:

$$p\left(\begin{bmatrix} \mathbf{x} \\ \mathbf{y} \end{bmatrix} | \Omega\right) = \frac{1}{(2\pi)^{n/2} \det(\Omega)^{-1/2}} \exp\left(-\frac{1}{2} \begin{bmatrix} \mathbf{x} \\ \mathbf{y} \end{bmatrix}^T \Omega \begin{bmatrix} \mathbf{x} \\ \mathbf{y} \end{bmatrix}\right). \quad (7)$$

The precision matrix Ω and the covariance matrix $\Sigma = \Omega^{-1}$ can be partitioned as follows [28], [35]:

$$\Omega = \begin{bmatrix} \Omega_{\mathbf{x}} & \Omega_{\mathbf{xy}} \\ \Omega_{\mathbf{yx}} & \Omega_{\mathbf{y}} \end{bmatrix} = \begin{bmatrix} \Sigma_{\mathbf{x}} & \Sigma_{\mathbf{xy}} \\ \Sigma_{\mathbf{yx}} & \Sigma_{\mathbf{y}} \end{bmatrix}^{-1} = \Sigma^{-1}. \quad (8)$$

Irrespective of the type of prediction (intra/inter), the MMSE prediction of \mathbf{x} from the reference samples in \mathbf{y} is

$$\mathbf{p} = \mathbb{E}[\mathbf{x}|\mathbf{y}] = \Sigma_{\mathbf{xy}} \Sigma_{\mathbf{y}}^{-1} \mathbf{y} = -\Omega_{\mathbf{x}}^{-1} \Omega_{\mathbf{xy}} \mathbf{y}, \quad (9)$$

and the resulting residual vector is $\mathbf{r} = \mathbf{x} - \mathbf{p}$ with covariance

$$\begin{aligned} \Sigma_{\mathbf{r}} &= \mathbb{E}[\mathbf{r}\mathbf{r}^T] = \mathbb{E}[(\mathbf{x} - \mathbf{p})(\mathbf{x} - \mathbf{p})^T] \\ &= \mathbb{E}[\mathbf{x}\mathbf{x}^T + \mathbf{p}\mathbf{p}^T - 2\mathbf{x}\mathbf{p}^T] \\ &= \Sigma_{\mathbf{x}} + \Sigma_{\mathbf{xy}} \Sigma_{\mathbf{y}}^{-1} \Sigma_{\mathbf{yx}} - 2\Sigma_{\mathbf{xy}} \Sigma_{\mathbf{y}}^{-1} \Sigma_{\mathbf{yx}} \\ &= \Sigma_{\mathbf{x}} - \Sigma_{\mathbf{xy}} \Sigma_{\mathbf{y}}^{-1} \Sigma_{\mathbf{yx}}. \end{aligned} \quad (10)$$

By the matrix inversion lemma [38], the precision matrix of the residual \mathbf{r} is shown to be equal to $\Omega_{\mathbf{x}}$, that is the submatrix in (8),

$$\Sigma_{\mathbf{r}}^{-1} = (\Sigma_{\mathbf{x}} - \Sigma_{\mathbf{xy}} \Sigma_{\mathbf{y}}^{-1} \Sigma_{\mathbf{yx}})^{-1} = \Omega_{\mathbf{x}}. \quad (11)$$

Since we also have $\Sigma_{\mathbf{x}} = (\Omega_{\mathbf{x}} - \Omega_{\mathbf{xy}} \Omega_{\mathbf{y}}^{-1} \Omega_{\mathbf{yx}})^{-1}$ by [38], the desired precision matrix can also be written as

$$\Omega_{\text{residual}} = \Sigma_{\mathbf{r}}^{-1} = \Omega_{\mathbf{x}} = \Sigma_{\mathbf{x}}^{-1} + \Omega_{\mathbf{xy}} \Omega_{\mathbf{y}}^{-1} \Omega_{\mathbf{yx}}. \quad (12)$$

This construction leads us to the following proposition formally stating the conditions for a residual signal (i.e., \mathbf{r}) to be modeled by an attractive GMRF.

Proposition 3. *Let the signals $\mathbf{x} \in \mathbb{R}^n$ and $\mathbf{y} \in \mathbb{R}^{n_p}$ be distributed based on the attractive GMRF model in (7) with precision matrix Ω . If the residual signal \mathbf{r} is estimated by minimum mean square error (MMSE) prediction of \mathbf{x} from \mathbf{y} (i.e., $\mathbf{r} = \mathbf{x} - \mathbb{E}[\mathbf{x}|\mathbf{y}]$), then the residual signal \mathbf{r} is distributed as an attractive GMRF whose precision matrix is a generalized graph Laplacian (i.e., Ω_{residual} in (12)).*

Proof. The proof follows from (7)–(12) where the inverse covariance of residual signal \mathbf{r} , $\Sigma_{\mathbf{r}}^{-1}$, is shown to be equal to $\Omega_{\mathbf{x}}$. Since $\Omega_{\mathbf{x}}$ is a submatrix of Ω in (8) and Ω is a GGL, $\Omega_{\text{residual}} = \Omega_{\mathbf{x}}$ is also a GGL. Hence, \mathbf{r} is distributed as an attractive GMRF whose precision is $\Omega_{\mathbf{x}}$. \square

Note that Proposition 3 also applies to the 1-D signal models presented in [2] which are special cases of (7).

B. Interpretation of Graph Weights for Predictive Transform Coding

Based on Proposition 3, the distribution of residual signals, denoted as $\mathbf{r} = [r_1 \ \cdots \ r_n]^T$, is defined by the following GMRF whose precision matrix is a GGL matrix \mathbf{L} (i.e., $\mathbf{L} = \Omega_{\text{residual}}$),

$$p(\mathbf{r}|\mathbf{L}) = \frac{1}{(2\pi)^{n/2} \det(\mathbf{L})^{-1/2}} \exp\left(-\frac{1}{2} \mathbf{r}^T \mathbf{L} \mathbf{r}\right), \quad (13)$$

where the quadratic term in the exponent can be decomposed in terms of graph weights (i.e., \mathbf{V} and \mathbf{W}) as

$$\mathbf{r}^T \mathbf{L} \mathbf{r} = \sum_{i=1}^n (\mathbf{V})_{ii} r_i^2 + \sum_{(i,j) \in \mathcal{I}} (\mathbf{W})_{ij} (r_i - r_j)^2 \quad (14)$$

such that $(\mathbf{W})_{ij} = -(\mathbf{L})_{ij}$, $(\mathbf{V})_{ii} = \sum_{j=1}^n (\mathbf{L})_{ij}$, and $\mathcal{I} = \{(i, j) | (v_i, v_j) \in \mathcal{E}\}$ is the set of index pairs of all vertices associated with the edge set \mathcal{E} .

Based on (13) and (14), it is clear that the distribution of the residual signal \mathbf{r} depends on edge weights (\mathbf{W}) and vertex weights (\mathbf{V}) where

- a model with larger (resp. smaller) edge weights (e.g., $(\mathbf{W})_{ij}$) increases the probability of having a smaller (resp. larger) squared difference between corresponding residual pixel values (e.g., r_i and r_j),
- a model with larger (resp. smaller) vertex weights (e.g., $(\mathbf{V})_{ii}$) increases the probability of pixel values (e.g., r_i) with smaller (resp. larger) magnitude.

In practice, a characterization of the edge and vertex weights (\mathbf{W} and \mathbf{V}) can be made by estimating \mathbf{L} from data, which depend on inherent signal statistics and the type of prediction used for predictive coding. We empirically investigate the graph weights associated with residual signals in Section VI.

C. DCTs/DSTs as GBTs Derived from Line Graphs

Some types of DCTs and DSTs, including DCT-2 and DST-7, are in fact special cases of GBTs derived from Laplacians of specific line graphs. The relation between different types of DCTs and graph Laplacian matrices is originally discussed in [39] where DCT-2 is shown to be equal to the GBT uniquely obtained from graph Laplacians of the following form:

$$\mathbf{L}_u = \begin{bmatrix} c & -c & & 0 \\ -c & 2c & -c & \\ & \ddots & \ddots & \ddots \\ & & -c & 2c & -c \\ 0 & & & -c & c \end{bmatrix} \text{ for } c > 0, \quad (15)$$

which represents uniformly weighted line graphs with no self-loops (i.e., all edge weights are equal to a positive constant and vertex weights to zero). Moreover, in [2], [40], it has been shown that DST-7 is the GBT derived from a graph Laplacian $\mathbf{L} = \mathbf{L}_u + \mathbf{V}$ where $\mathbf{V} = \text{diag}([c \ 0 \ \dots \ 0]^T)$ including a self-loop at vertex v_1 with weight $f_v(v_1) = c$. Based on the results in [39], [41], various other types of DCTs and DSTs can be characterized using graphs. Table II specifies the line graphs (with n vertices v_1, v_2, \dots, v_n having self-loops at v_1 and v_n) corresponding to different types of DCTs and DSTs, which are GBTs derived from graph Laplacians of the form $\tilde{\mathbf{L}} = \mathbf{L}_u + \tilde{\mathbf{V}}$ where $\tilde{\mathbf{V}} = \text{diag}([f_v(v_1) \ 0 \ \dots \ 0 \ f_v(v_n)]^T)$.

TABLE II
DCTs/DSTs CORRESPONDING TO $\tilde{\mathbf{L}}$ WITH DIFFERENT VERTEX WEIGHTS.

Vertex weights	$f_v(v_1)=0$	$f_v(v_1)=c$	$f_v(v_1)=2c$
$f_v(v_n)=0$	DCT-2	DST-7	DST-4
$f_v(v_n)=c$	DCT-8	DST-1	DST-6
$f_v(v_n)=2c$	DCT-4	DST-5	DST-2

The current state-of-the-art VVC standard [9] uses separable transforms specified by pairs of DCT-2, DST-7 and DCT-8, that can be viewed as GBSTs. The GBST designs proposed in this paper are also based on line graphs whose weights, unlike those of the DCTs/DSTs, are learned from data.

IV. GRAPH LEARNING FOR GRAPH-BASED TRANSFORM DESIGN

A. Generalized Graph Laplacian Estimation

As justified in Proposition 3, the residual signal $\mathbf{r} \in \mathbb{R}^n$ is modeled as an attractive GMRF, $\mathbf{r} \sim \mathcal{N}(\mathbf{0}, \Sigma = \mathbf{L}^{-1})$, whose precision matrix is a GGL denoted by \mathbf{L} . Assuming that we have k residual signals, $\mathbf{r}_1, \dots, \mathbf{r}_k$, sampled from $\mathcal{N}(\mathbf{0}, \Sigma = \mathbf{L}^{-1})$, the likelihood of a candidate \mathbf{L} is

$$\prod_{i=1}^k p(\mathbf{r}_i | \mathbf{L}) = (2\pi)^{-\frac{kn}{2}} \det(\mathbf{L})^{\frac{k}{2}} \prod_{i=1}^k \exp\left(-\frac{1}{2} \mathbf{r}_i^T \mathbf{L} \mathbf{r}_i\right). \quad (16)$$

The maximization of the likelihood in (16) can be equivalently formulated as minimizing the negative log-likelihood, that is

$$\begin{aligned} \hat{\mathbf{L}}_{\text{ML}} &= \underset{\mathbf{L}}{\text{argmin}} \left\{ \frac{1}{2} \sum_{i=1}^k \text{Tr}(\mathbf{r}_i^T \mathbf{L} \mathbf{r}_i) - \frac{k}{2} \log \det(\mathbf{L}) \right\} \\ &= \underset{\mathbf{L}}{\text{argmin}} \{ \text{Tr}(\mathbf{L} \mathbf{S}) - \log \det(\mathbf{L}) \} \end{aligned} \quad (17)$$

where $\mathbf{S} = \frac{1}{k} \sum_{i=1}^k \mathbf{r}_i \mathbf{r}_i^T$ is the sample covariance, and $\hat{\mathbf{L}}_{\text{ML}}$ denotes the maximum likelihood (ML) estimate of \mathbf{L} . To find the best GGL from a set of residual signals $\{\mathbf{r}_1, \dots, \mathbf{r}_k\}$ in a maximum likelihood sense, we solve the following GGL estimation problem with connectivity constraints:

$$\begin{aligned} &\underset{\mathbf{L} \succeq 0}{\text{minimize}} \quad \text{Tr}(\mathbf{L} \mathbf{S}) - \log \det(\mathbf{L}) \\ &\text{subject to} \quad (\mathbf{L})_{ij} \leq 0 \quad \text{if } (\mathbf{A})_{ij} = 1 \\ &\quad \quad \quad (\mathbf{L})_{ij} = 0 \quad \text{if } (\mathbf{A})_{ij} = 0 \end{aligned} \quad (18)$$

where \mathbf{S} denotes the sample covariance of residual signals, and \mathbf{A} is the connectivity matrix representing the graph structure (i.e., the set of graph edges). In order to optimally solve (18), we use the *GGL estimation algorithm* proposed in our previous work on graph learning [25], [42].

B. Graph-based Transform Design

To design separable and nonseparable GBTs (GBSTs and GBNTs), we solve instances of (18) denoted as $\text{GGL}(\mathbf{S}, \mathbf{A})$ with different connectivity constraints represented by \mathbf{A} . Then, the optimized GGL matrices are used to derive GBTs.

Graph learning oriented GBST (GL-GBST). For the GL-GBST design, we solve two instances of (18) to optimize two separate line graphs used to derive \mathbf{U}_{row} and \mathbf{U}_{col} in (5). Since we wish to design a separable transform, each line graph can be optimized independently³. Thus, our basic goal is finding the best line graph pair based on sample covariance matrices \mathbf{S}_{row} and \mathbf{S}_{col} created from rows and columns of residual block signals. For $N \times N$ residual blocks, the proposed GL-GBST construction has the following steps:

- 1) Create the connectivity matrix \mathbf{A}_{line} representing a line graph structure with $n = N$ vertices as in Fig. 2.
- 2) Obtain two $N \times N$ sample covariances, \mathbf{S}_{row} and \mathbf{S}_{col} , from rows and columns of size N , respectively, obtained from residual blocks in the dataset.
- 3) Solve instances of the problem in (18), $\text{GGL}(\mathbf{S}_{\text{row}}, \mathbf{A}_{\text{line}})$ and $\text{GGL}(\mathbf{S}_{\text{col}}, \mathbf{A}_{\text{line}})$, by using the GGL estimation algorithm [25] to learn Laplacians \mathbf{L}_{row} and \mathbf{L}_{col} representing line graphs, respectively.
- 4) Perform eigendecomposition on \mathbf{L}_{row} and \mathbf{L}_{col} to obtain GBTs, \mathbf{U}_{row} and \mathbf{U}_{col} , which define the GBST as in (5).

Graph learning oriented GBNT (GL-GBNT). Similarly, for $N \times N$ residual block signals, we propose the following steps to design a GL-GBNT:

- 1) Create the connectivity matrix \mathbf{A} based on a desired graph structure supporting $n = N^2$ vertices. In this paper, we

³Alternatively, joint optimization of the transforms associated with rows and columns has been proposed in [43], [44].

use connectivity constraints based on grid graphs⁴, as illustrated in Fig. 3.

- 2) Obtain $N^2 \times N^2$ sample covariance \mathbf{S} using residual block signals in the dataset (after vectorizing the block signals).
- 3) Solve the problem $\text{GGL}(\mathbf{S}, \mathbf{A})$ by using the GGL estimation algorithm [25] to estimate a Laplacian \mathbf{L} .
- 4) Perform eigendecomposition on \mathbf{L} to obtain the $N^2 \times N^2$ GBNT, \mathbf{U} defined in (6).

C. Computational complexity of GL-GBTs

In practice, GL-GBTs do not introduce an additional computational complexity over other transform types implemented using full-matrix multiplications⁵. The recent work in [45] also empirically demonstrates that GL-GBSTs do not increase encoder/decoder run-time over VVC [9], if they are used to replace the separable transforms derived from DST-7 and DCT-8. However, it is important to note that nonseparable transforms (such as the ones in VVC) are inherently complex as they require N^2 multiplications per pixel for an $N \times N$ block signal, while separable transforms only need $2N$ multiplications per pixel. To alleviate the complexity of nonseparable transforms, the methods providing low-complexity approximations or decompositions in [16], [43], [46] can be applied instead of using full-matrix multiplications.

D. Theoretical Justification for GL-GBTs

It has been shown that KLT is optimal for transform coding of jointly Gaussian sources in terms of mean-square error (MSE) criterion under high-bitrate assumptions [47]–[49]. Since GMRF models lead to jointly Gaussian distributions, the corresponding KLTs are optimal in theory. However, in practice, a KLT is obtained by eigendecomposition of the associated sample covariance, which has to be estimated from a training dataset where the number of data samples may not be sufficient to accurately recover the parameters. As a result, the sample covariance may lead a poor estimation of the actual model parameters [22], [23]. To improve estimation accuracy and alleviate overfitting, it is often useful to reduce the number of model parameters by introducing model constraints and regularization. From the statistical learning theory perspective [50], [51], the advantage of our proposed GL-GBT over KLT is that KLT requires learning $O(n^2)$ model parameters while GL-GBT only needs $O(n)$, given the connectivity constraints in (18). Therefore, our graph learning approach provides better *generalization* in learning the signal model by taking into account variance-bias tradeoff. This advantage can also be justified based on the following error bounds characterized in [23], [52]. Assuming that k residual blocks are used for calculating the sample covariance \mathbf{S} , under general set of assumptions, the error bound for estimating Σ with \mathbf{S} derived in [52] is

$$\|\Sigma - \mathbf{S}\|_F = O\left(\sqrt{\frac{n^2 \log(n)}{k}}\right), \quad (19)$$

⁴According to our experiments across different prediction modes, using grid graph constraints led to a better coding efficiency as compared to using constraints that further allow edges between the nearest diagonal pixels.

⁵In VVC [9], the adopted variant of nonseparable transforms in [15] as well as the DST-7 and DCT-8 are implemented using full-matrix multiplications.

while estimating the precision matrix Ω by using the proposed graph learning approach leads to the following bound shown in [23],

$$\|\Omega - \mathbf{L}\|_F = O\left(\sqrt{\frac{n \log(n)}{k}}\right), \quad (20)$$

where \mathbf{L} denotes the estimated GGL. Thus, in terms of the worst-case errors (based on Frobenius norm), the proposed method provides a better model estimation as compared to the estimation based on the sample covariance. Section VII empirically justifies the advantage of GL-GBT against KLT.

V. EDGE-ADAPTIVE GRAPH-BASED TRANSFORMS

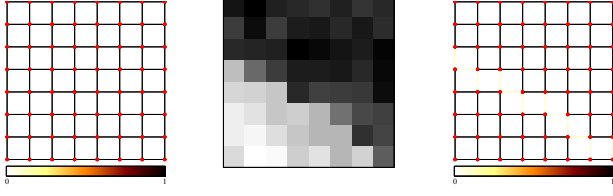
The optimality of GL-GBTs relies on the assumption that the residual signal characteristics are the same across different blocks. However, in practice, video blocks often exhibit complex image edge structures that can degrade the coding performance when the transforms are designed from average statistics without any classification based on image edges. In order to achieve better compression for video signals with image edges, we propose edge-adaptive GBTs (EA-GBTs), designed on a per-block basis, by constructing a graph whose weights are determined based on the salient image edges in each residual block.

A. EA-GBT Construction

To design an EA-GBT for a residual block, we first detect image edges based on a threshold T_{edge} applied on gradient values, obtained using the *Prewitt* operator on the block. Then, edge weights of a predefined graph are modified according to the locations of detected image edges, and the resulting graph is used to derive the associated GBT. As depicted in Fig. 4, to construct a graph, we start with a uniformly weighted grid graph for which all edge weights are equal to a fixed constant w_c (Fig. 4a). Then, the detected image edges on a given residual block (Fig. 4b) are used to determine the co-located edges in the graph, and the corresponding weights are reduced as $w_e = w_c / s_{\text{edge}}$ (Fig. 4c), where $s_{\text{edge}} \geq 1$ is a parameter modeling the sharpness of image edges (i.e., the level of differences between pixel values in presence of an image edge). Thus, a larger s_{edge} leads to smaller weights on edges connecting pixels (vertices) with an image edge in between.

According to our simulations on residual data, coding gains are observed for $s_{\text{edge}} > 10$, which empirically corresponds to residuals with an intensity difference of at least 12 (between pixels adjacent to an image edge)⁶. In our experiments, a conservative threshold of $T_{\text{edge}} = 10$ is used for image edge detection, and the parameter s_{edge} is set to 10. Although the proposed EA-GBT design can be extended with multiple s_{edge} parameters, our experiments showed that such extensions do not provide a good rate-distortion trade-off due to the additional signaling overhead. For efficient signaling of detected edges, we employ arithmetic edge coding (AEC) [53], a state-of-the-art binary edge-map codec.

⁶Residual signals are in 9-bit signed integer precision, since the input video sequences used in our experiments are all in 8-bit unsigned integer precision.



(a) Initial graph (b) Residual block signal (c) Constructed graph

Fig. 4. An illustration of graph construction for a given 8×8 residual block signal where $w_c = 1$ and $w_e = w_c/s_{\text{edge}} = 0.1$ where $s_{\text{edge}} = 10$.

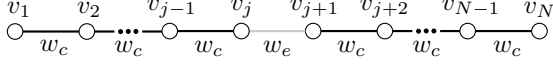


Fig. 5. A 1-D graph-based model with an image edge at location $l = j$. All black colored edges have weights equal to w_c , and the gray edge between vertices v_j and v_{j+1} is weighted as $w_e = w_c/s_{\text{edge}}$.

From the compression perspective, the EA-GBT construction can also be viewed as a classification procedure, so that each residual block (e.g., in Fig. 4b) is assigned to a class of signals associated with an attractive GMRF, whose corresponding graph (i.e., GGL) is determined by s_{edge} and image edge detection based on T_{edge} (e.g., in Fig. 4c). By using attractive GMRFs, the following subsection theoretically validates our experimental observation of achieving coding gains for $s_{\text{edge}} > 10$.

B. Computational complexity of EA-GBTs

As GL-GBTs, EA-GBTs need to be implemented based on full-matrix multiplications, whose implications on complexity are discussed in Section IV-C. Moreover, block-adaptive coding schemes such as [30]–[32] and EA-GBT introduce an additional computational overhead since transforms need to be constructed on a per-block basis. In practice, this additional complexity can be eliminated for EA-GBT by using a pre-determined set of graphs (such as graph templates introduced in [1]) capturing a fixed number of image edge patterns in an RDOT scheme, where the associated GBTs are stored and not constructed per-block. In this paper, in order to evaluate the best case performance of EA-GBT we do not impose any restrictions on the image-edge patterns and evaluate the coding efficiency of EA-GBT as a block-adaptive scheme.

C. Theoretical Justification for EA-GBTs

We present a theoretical justification for advantage of EA-GBTs over KLTs. For the sake of simplicity, our analysis is based on 1-D models with a single image edge, whose the location l is uniformly distributed as

$$P(l = j) = \begin{cases} \frac{1}{N-1} & \text{for } j = 1, \dots, N-1 \\ 0 & \text{otherwise} \end{cases} \quad (21)$$

where N is the number of pixels (i.e., vertices) on the line graph depicted in Fig. 5. This construction leads to a Gaussian mixture distribution based on $M = N - 1$ attractive GMRFs,

$$p(\mathbf{x}) = \sum_{j=1}^M P(l = j) N(\mathbf{0}, \Sigma_j) \quad (22)$$

with Σ_j denoting the covariance of the j -th attractive GMRF, whose corresponding graph has an image edge between pixels

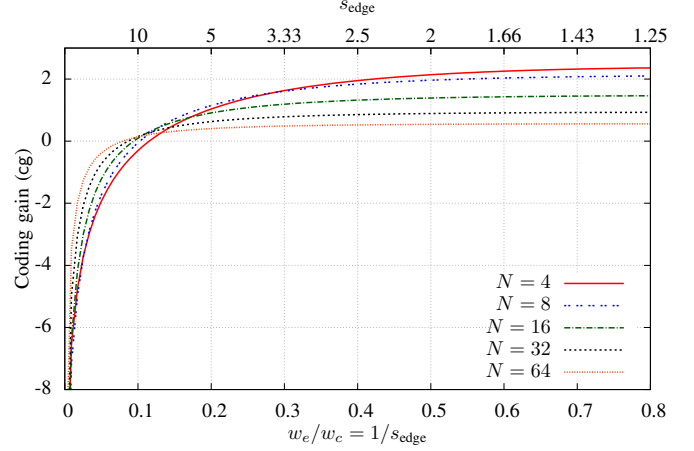


Fig. 6. Coding gain (cg) versus s_{edge} for block sizes with $N = 4, 8, 16, 32, 64$. EA-GBT provides better coding gain (i.e., cg is negative) when s_{edge} is larger than 10 across different block sizes.

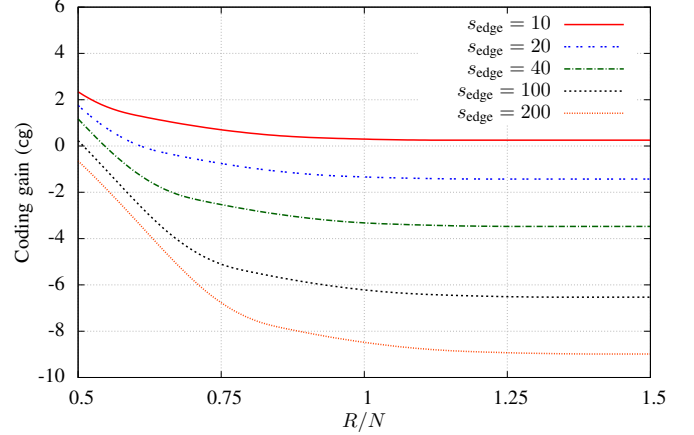


Fig. 7. Coding gain (cg) versus bits per pixel (R/N) for different edge sharpness parameters $s_{\text{edge}} = 10, 20, 40, 100, 200$. EA-GBT provides better coding gain (i.e., cg is negative) if s_{edge} is larger than 10 for different block sizes.

v_j and v_{j+1} as illustrated in Fig. 5. Since \mathbf{x} follows a Gaussian mixture distribution, the KLT obtained from the covariance of \mathbf{x} (which implicitly performs a second-order approximation of the distribution) is suboptimal in MSE sense [54]. Especially, with many possible image edge locations and different orientations, the underlying distribution may contain a large number of mixtures (i.e., a large M), which makes learning a model from average statistics inefficient. On the other hand, the proposed EA-GBT removes the uncertainty due to the random variable l by detecting the location of the image edge in pixel (vertex) domain, and then constructing a GBT based on the detected image edge. Yet, EA-GBT requires allocating additional bits to represent the image edge (side) information, while KLT only allocates bits for coding transform coefficients.

To demonstrate the rate-distortion tradeoff between KLT and EA-GBT based coding schemes, we use classical rate-distortion theory results with high-bitrate assumptions [47]–[49], in which the distortion (D) can be written as a function of bitrate (R),

$$D(\bar{R}) = \frac{N}{12} 2^{2\bar{H}_d} 2^{-2\bar{R}} \quad (23)$$

with

$$\bar{R} = \frac{R}{N} \quad \text{and} \quad \bar{H}_d = \frac{1}{N} \sum_{i=1}^N H_d((\mathbf{c})_i) \quad (24)$$

where R denotes the total bitrate allocated to code transform coefficients in $\mathbf{c} = \mathbf{U}^T \mathbf{x}$, and $H_d((\mathbf{c})_i)$ is the differential entropy of transform coefficient $(\mathbf{c})_i$. For EA-GBT, R is allocated to code both transform coefficients ($R_{\text{EA-GBT}}^{\text{coeff}}$) and side information (R^{edge}), so we have

$$R = R_{\text{EA-GBT}}^{\text{coeff}} + R^{\text{edge}} = R_{\text{EA-GBT}}^{\text{coeff}} + \log_2(M) \quad (25)$$

while for KLT, the bitrate is allocated only to code transform coefficients ($R_{\text{KLT}}^{\text{coeff}}$), so that $R = R_{\text{KLT}}^{\text{coeff}}$. Fig. 6 shows the coding gain of EA-GBT over KLT for different sharpness parameters (i.e., s_{edge}) in terms of the following metric, called coding gain,

$$\text{cg}(D_{\text{EA-GBT}}, D_{\text{KLT}}) = 10 \log_{10} \left(\frac{D_{\text{EA-GBT}}}{D_{\text{KLT}}} \right) \quad (26)$$

where $D_{\text{EA-GBT}}$ and D_{KLT} denote distortion levels measured at high-bitrate regime for EA-GBT and KLT, respectively. EA-GBT provides better compression for negative cg values in Fig. 6 which appear when the sharpness of edges s_{edge} is large (e.g., $s_{\text{edge}} > 10$).

Note that the distortion function in (23) is derived based on high-bitrate assumptions. To characterize rate-distortion tradeoff for different bitrates, we employ the reverse water-filling technique [47], [55] by varying the parameter θ in (28) to obtain rate and distortion measures as follows

$$R(D) = \sum_{i=1}^N \frac{1}{2} \log_2 \left(\frac{\lambda_i}{D_i} \right) \quad (27)$$

where λ_i is the i -th eigenvalue of the signal covariance, and

$$D_i = \begin{cases} \lambda_i & \text{if } \lambda_i \geq \theta \\ \theta & \text{if } \theta < \lambda_i \end{cases} \quad (28)$$

so that $D = \sum_{i=1}^N D_i$. The rate ($R(D)$) and distortion (D) for KLT are estimated based on the covariance associated with (22). For EA-GBT, they are averaged over the metrics obtained for M covariances (i.e., Σ_j for $j = 1, \dots, M$), as their frequency of occurrence follows the uniform distribution in (21).

Figure 7 illustrates the coding gain formulated in (26) achieved at different bitrates, where each curve correspond to a different s_{edge} parameter. Similar to Fig. 6, EA-GBT leads to a better compression if the sharpness of edges, s_{edge} , is large (e.g., $s_{\text{edge}} > 10$ for $R/N > 0.6$)⁷. At low-bitrates (e.g., $R/N < 0.6$), EA-GBT can perform worse than KLT for $s_{\text{edge}} = 20, 40$, yet EA-GBT outperforms as bitrate increases.

VI. RESIDUAL BLOCK SIGNAL CHARACTERISTICS AND GRAPH-BASED MODELS

In this section, we discuss statistical characteristics of intra and inter predicted residual blocks, and empirically justify our theoretical analysis and observations in Section III. Our empirical results are based on residual signals obtained by encoding 5 different video sequences (*City*, *Crew*, *Harbour*, *Soccer* and *Parkrun* [56]) using the HEVC reference software (HM-14)

[6] at 4 different QP parameters ($QP = \{22, 27, 32, 37\}$). Although the HEVC standard does not implement optimal MMSE prediction (which is the main assumption in Section III), it includes 35 intra and 8 inter prediction modes, which provide reasonably good prediction for different classes of block signals.

Figs. 8–13 depict statistical characteristics of 8×8 residual signals for a few intra and inter prediction modes⁸. In these figures, sample variances of residuals and corresponding graph-based models are illustrated. Both grid and line graphs with normalized edge and vertex weights⁹ are estimated from residual data by solving the GGL estimation problem in (18) used for GL-GBNT and GL-GBST construction.

Naturally, residual blocks have different statistical characteristics depending on the type of prediction and the prediction mode. The sample variances shown in Figs. 8a–13a for different prediction modes lead us to the following observations:

- As expected, inter predicted blocks have smaller sample variance (energy) across pixels compared to intra predicted blocks, because inter prediction provides better prediction with larger number of reference pixels as shown in Fig. 3.
- In intra prediction, sample variances are generally larger at the bottom-right part of residual blocks, since reference pixels are located at the top and left of a block where the prediction is relatively better. This holds specifically for planar, DC and diagonal modes using pixels on both top and left as references for prediction.
- For some angular modes including intra horizontal/vertical mode, only left/top pixels are used as references. In such cases the sample variance gets larger as distance from reference pixels increases. Fig. 10a illustrates sample variances corresponding to the horizontal mode.
- In inter prediction, sample variances are larger around the boundaries and corners of the residual blocks mainly because of occlusions leading to partial mismatches between reference and predicted blocks.
- In inter prediction, PU partitions lead to larger residual energy around the partition boundaries as shown in Fig. 13a corresponding to horizontal PU partitioning ($N \times 2N$).

Moreover, inspection of the estimated graphs in Figs. 8–13 leads to following observations, which validate our theoretical analysis and justify the interpretation of model parameters in terms of graph weights discussed in Section III:

- Irrespective of the prediction mode/type, vertex (self-loop) weights tend to be larger for the pixels that are connected to reference pixels. Specifically, in intra prediction, graphs have larger vertex weights for vertices (pixels) located at the top and/or left boundaries of the block (Figs. 8–11), while the vertex weights are approximately uniform across vertices in inter prediction (Figs. 12 and 13).
- In intra prediction, the grid and line graphs associated with planar and DC modes are similar in structure (Figs. 8 and 9), where their edge weights decrease as the distance of

⁸For 4×4 and 16×16 residual blocks, the structure of sample variances and graphs are quite similar to the ones in Figs. 8a–13a.

⁹Section II formally defines edge and vertex weights, denoted by $(\mathbf{W})_{ij} = (\mathbf{W})_{ji} = f_w((v_i, v_j))$ and $(\mathbf{V})_{ii} = f_v(v_i)$, used for deriving GGLs.

⁷In practice, $R/N > 0.6$ is typically achieved at quantization parameters [6] smaller than 32 in video video coding.

edges to the reference pixels increase. Also, vertex weights are larger for the pixels located at top and left boundaries, since planar and DC modes use reference pixels from the both sides (top and left). These observations indicate that the prediction performance gradually decreases for pixels increasingly farther away from the reference pixels.

- For intra prediction with horizontal mode (Fig. 10), the grid graph has larger vertex weights at the left boundary of the block. This is because the prediction only uses reference pixels on the left side of the block. Therefore, the line graph associated to rows has a large self-loop at the first pixel, while the other line graph has no dominant vertex weights. However, grid and line graphs for the diagonal mode (Fig. 11), are more similar to the ones for planar and DC modes, since the diagonal mode also uses the references from both top and left sides.
- For inter prediction with PU mode $2N \times 2N$ (do not perform any partitioning), the graph weights (both vertex and edge weights) are approximately uniform across the different edges and vertices (Fig. 12). This shows that the prediction performance is similar at different locations (pixels). In contrast, the graphs for the PU mode $N \times 2N$ (performs horizontal partitioning) leads to smaller edge weights around the PU partitioning (Fig. 13). In the grid graph, we observe smaller weights between the partitioned vertices. Among line graphs, only the line graph designed for columns has a small weight in the middle, as expected.

VII. EXPERIMENTAL RESULTS

A. Experimental Setup

In our experiments, we generate two residual block datasets, one for training and the other for testing. The residual blocks (samples of r as shown in Fig. 1 at the encoder side) are collected by using the encoder implemented in HEVC reference software (HM version 14)¹⁰ [6], where both datasets are created by encoding the training and test video sequences at four different quantization parameters QPs from $\{22, 27, 32, 37\}$ as specified in [57]. For the training dataset, residual blocks are obtained by encoding five video sequences, *City*, *Crew*, *Harbour*, *Soccer* and *Parkrun*, and for the test dataset, we use another five video sequences, *BasketballDrill*, *BQMall*, *Mobcal*, *Shields* and *Cactus* [56], [57]. In both datasets, transform block sizes are restricted to 4×4 , 8×8 and 16×16 , and each residual block is classified (labeled) using the mode and block size information determined by the HM encoder after RD optimization. Specifically, intra predicted blocks are classified based on 35 intra prediction modes offered in HEVC. Similarly, inter predicted blocks are classified based on 7 different prediction unit (PU) partitions, such that 2 square PU partitions are grouped as one class and other 6 rectangular PU partitions determine other classes. Hence, datasets consist of $35 + 7 = 42$ classes in total. For each combination of 42 classes and block sizes (4×4 , 8×8 and 16×16), the optimal

GL-GBSTs, GL-GBNTs and nonseparable KLTs are designed offline using the residual blocks in the training dataset. As designing separate sets of transforms per QP does not improve the coding performance based on our experiments, a single set of transforms (per class and block size) is designed for all QPs without splitting the training dataset for each QP. On the other hand, EA-GBTs are constructed on a per-block basis based on the detected image edges. The details of transform construction are discussed in Sections IV and V.

In order to solely evaluate the effect of transforms on coding performance, transform coding is performed out of the HM encoding loop¹¹ while retaining all the other coding decisions made by HM on partitioning, prediction and filtering. Note that all transforms are compared based on rate-distortion performance on the *same* residual data. That is, we generate residual data first using HM and then compare the performance of DCT, KLT and GBT on those residuals. In our experimental setup, the transform coding first applies designated transforms (e.g., DCT or GBT) on the residual blocks, associated with a given QP in the test dataset, then the resulting transform coefficients are uniformly quantized using the same quantization step size derivation in HM (derived from QP) and entropy coded using arithmetic coding [60] to generate bitstreams. The proposed and baseline transforms are tested on mode-dependent transform (MDT) and rate-distortion optimized transform (RDOT) schemes. Specifically, the MDT scheme assigns a single GBT/KLT trained for each class/mode and block size. The RDOT scheme selects the best transform from a predefined set of transforms, denoted as \mathcal{T} , by minimizing the rate-distortion cost $J(\lambda_{rd}) = D + \lambda_{rd}R$ [61] where the multiplier $\lambda_{rd} = 0.85 \times 2^{(QP-12)/3}$ [6] depends on the QP parameter. In our RDOT experiments, all transform sets include DCT in addition to a GL-GBT (trained per-class and per-block size) or an EA-GBT (constructed per-block). Any side information needed to determine transforms (at the decoder side) are included in the bitstreams as signaling overhead. In the RDOT scheme, the transform index is signalled using truncated unary codes [9]¹². If the encoder chooses EA-GBT, the necessary graph (i.e., image edge) information is further sent by using the arithmetic edge encoder (AEC) [53].

The compression performance across different bitrate operating points is measured using Bjontegaard-delta rate (BD-rate) [62] metric by performing the transform coding experiments at QPs 22, 27, 32 and 37.

B. Compression Results

Table III presents the overall coding gains achieved by using KLTs, GL-GBSTs and GL-GBNTs with MDT and RDOT schemes for intra and inter predicted blocks. According to the results, GL-GBNT outperforms KLT irrespective of the prediction type and coding scheme. Fig. 14 further demonstrates the advantage of proposed approach over KLT when fewer number of training samples are available, where

¹⁰HM-14 was the latest version at that time when datasets were generated and also used in our previous work [1], [2]. HM-14 implements all normative functionalities of HEVC and the changes between HM-14 and the current latest version (HM-16) are incremental.

¹¹The simulation setups in [30], [32], [58], [59] are a few examples where experiments are conducted out of the encoding loop. Our setup specifically decouples the transform coding part from the rest of the HM encoding loop.

¹²Note that MDT does not require any signaling for transforms, because a single transform is available per-mode.

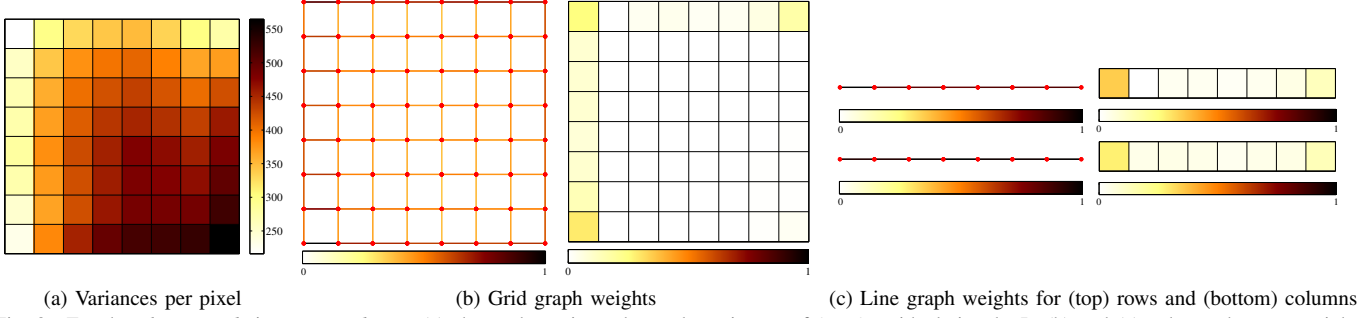


Fig. 8. For the *planar mode* in *intra prediction* (a) shows the estimated sample variances of 8×8 residual signals. In (b) and (c), edge and vertex weights are shown for grid and line graphs learned from residual data, respectively. Darker colors represent larger values.

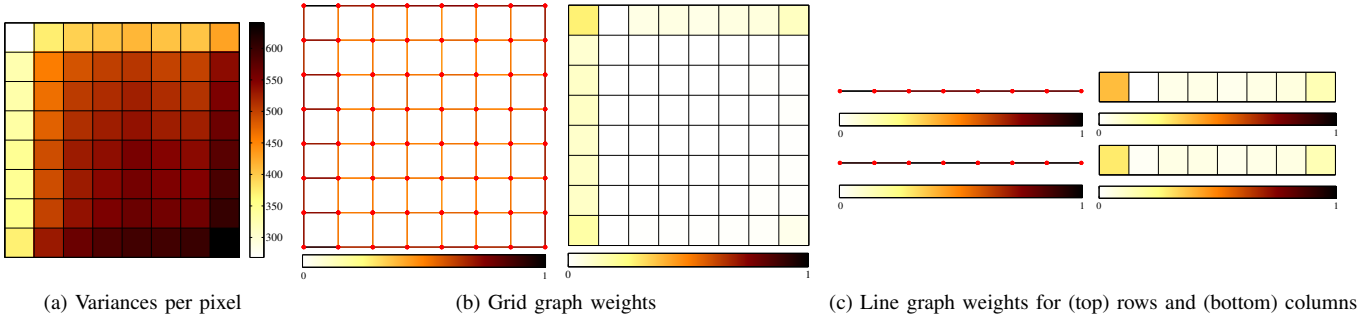


Fig. 9. For the *DC mode* in *intra prediction* (a) shows the estimated sample variances of 8×8 residual signals. In (b) and (c), edge and vertex weights are shown for grid and line graphs learned from residual data, respectively. Darker colors represent larger values.

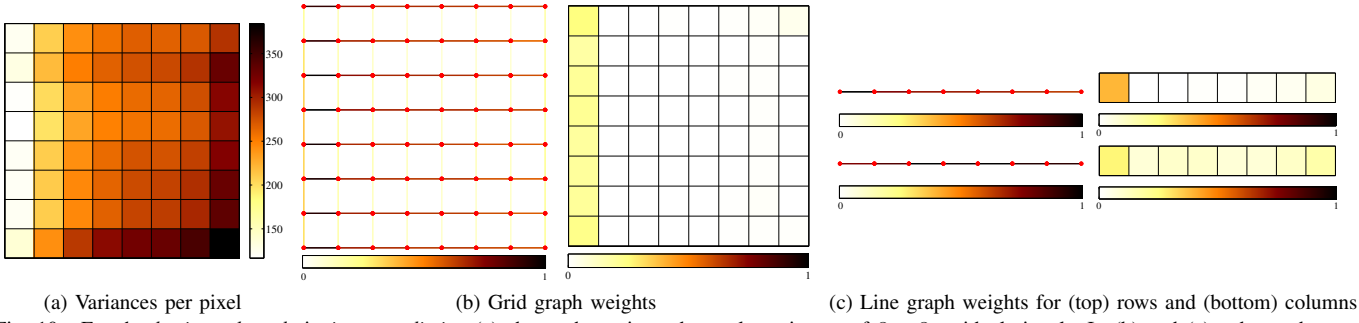


Fig. 10. For the *horizontal mode* in *intra prediction* (a) shows the estimated sample variances of 8×8 residual signals. In (b) and (c), edge and vertex weights are shown for grid and line graphs learned from residual data, respectively. Darker colors represent larger values.

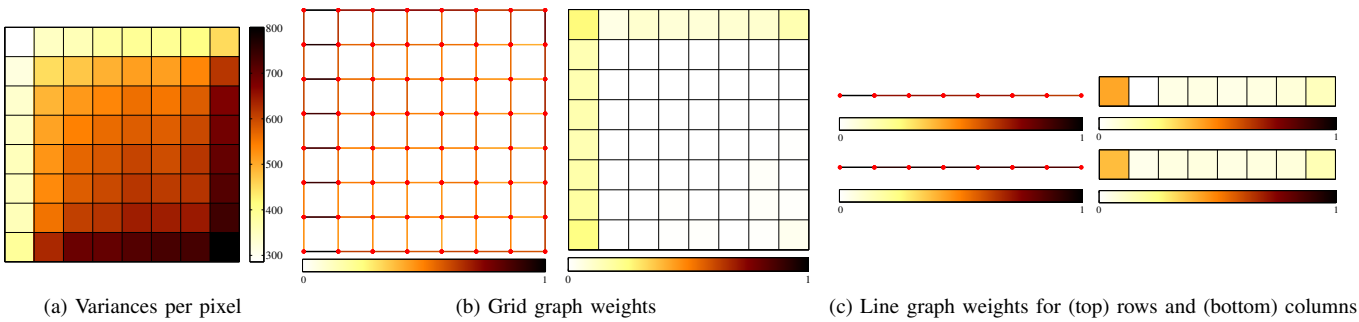


Fig. 11. For the *diagonal mode* in *intra prediction* (a) shows the estimated sample variances of 8×8 residual signals. In (b) and (c), edge and vertex weights are shown for grid and line graphs learned from residual data, respectively. Darker colors represent larger values.

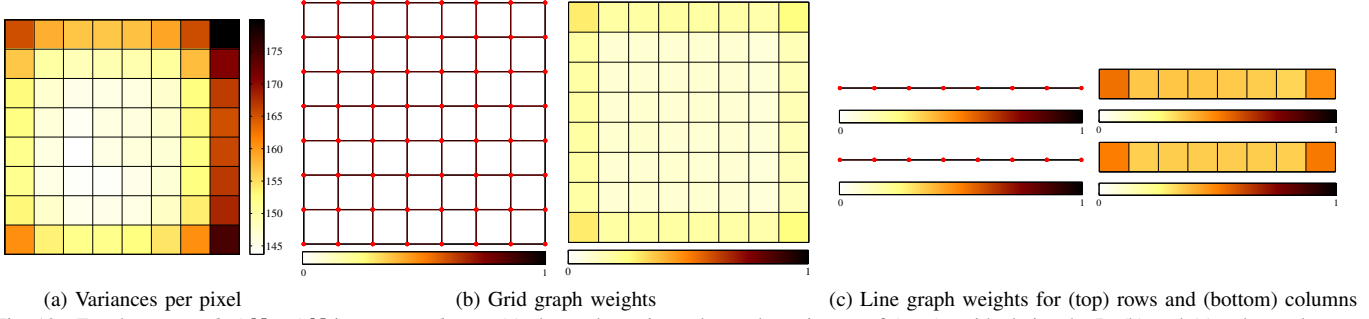


Fig. 12. For the *PU mode* $2N \times 2N$ in *inter prediction* (a) shows the estimated sample variances of 8×8 residual signals. In (b) and (c), edge and vertex weights are shown for grid and line graphs learned from residual data, respectively. Darker colors represent larger values.

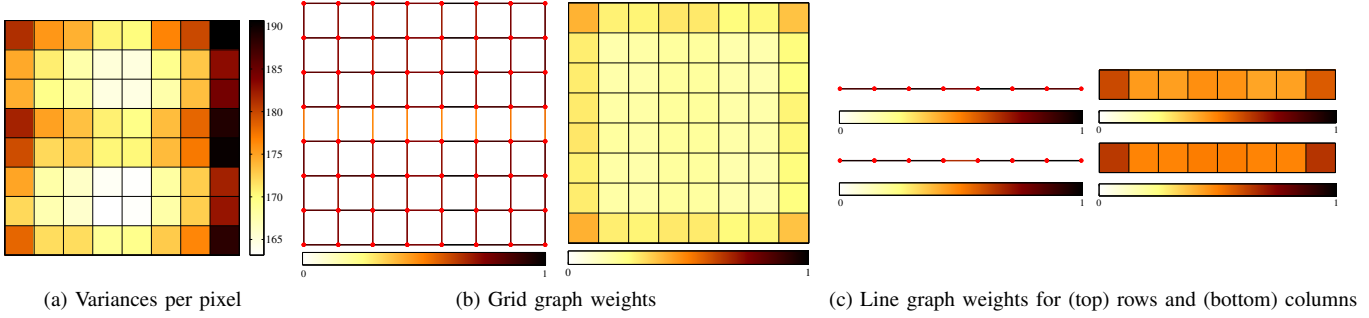


Fig. 13. For the *PU mode* $N \times 2N$ in *inter prediction* (a) shows the estimated sample variances of 8×8 residual signals. In (b) and (c), edge and vertex weights are shown for grid and line graphs learned from residual data, respectively. Darker colors represent larger values.

the performance difference between GL-GBNT and KLT is increased as the number of available training samples are reduced. Specifically, the BD-rate gap between GL-GBNT and KLT increases from 0.7% to 1.5% when twenty-percent of the training data is used instead of the complete data. This validates our observation that the proposed graph learning method leads to a more robust transform and provides a better generalization than KLT. Table III also shows that GL-GBNT performs substantially better than GL-GBST for coding intra predicted blocks, while for inter blocks GL-GBST performs slightly better than GL-GBNT. This is because, inter predicted residuals tend to have a separable structure as shown in Figs. 12 and 13, yet intra residuals have more directional structures as shown in Figs. 8, 9 and 11, which are better captured by using non-separable transforms. Moreover, RDOT scheme significantly outperforms MDT, since RDOT has multiple transform candidates providing a better adaptation to different block characteristics with RD optimization, while MDT offers a single transform per-mode¹³. Naturally, this coding gain comes at a cost for encoders as they need to search for the additional transform mode, which increased the encoder run-time about 10% and has no run-time impact at the decoder in our experiments.

Table IV compares the RDOT coding performance of KLTs, GL-GBSTs and GL-GBNTs on residual blocks with different prediction modes. In RDOT scheme the transform sets are $\mathcal{T}_{\text{KLT}} = \{\text{DCT}, \text{KLT}\}$, $\mathcal{T}_{\text{GL-GBST}} = \{\text{DCT}, \text{GL-GBST}\}$ and

¹³In our RDOT experiments on intra predicted residuals, GL-GBNT is selected 62% of the time against DCT for the diagonal mode, while GL-GBNT is selected 33% of the time for the DC mode. This indicates that per-mode block characteristics can significantly differ, where residuals obtained from certain modes (such as DC) can be better captured with DCT.

TABLE III
COMPARISON OF KLT, GL-GBST AND GL-GBNT WITH MDT AND RDOT SCHEMES IN TERMS OF BD-RATE (% BITRATE REDUCTION) WITH RESPECT TO THE DCT. SMALLER (NEGATIVE) BD-RATES MEAN BETTER COMPRESSION.

Transform	Intra Prediction		Inter Prediction	
	MDT	RDOT	MDT	RDOT
KLT	-1.81	-6.02	-0.09	-3.28
GL-GBST	-1.16	-4.61	-0.25	-3.89
GL-GBNT	-2.04	-6.70	-0.18	-3.68

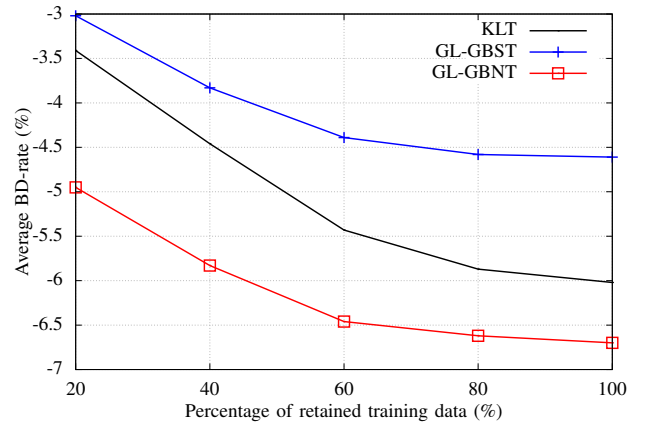


Fig. 14. BD-rates achieved for coding intra predicted blocks with the RDOT scheme based on KLT, GL-GBST and GL-GBNT, which are trained on datasets with fewer number of samples. This experiment is conducted by randomly sampling 20%, 40%, 60% and 80% of the data from the original dataset and repeated 20 times to estimate average BD-rates. The BD-rates at 100% correspond to the results in Table III where the complete training dataset is used.

$\mathcal{T}_{\text{GL-GBNT}} = \{\text{DCT}, \text{GL-GBNT}\}$, which consist of DCT and a trained transform for each mode and block size. The results show that GL-GBNT consistently outperforms KLT for all prediction modes. Similar to Table III, GL-GBST provides slightly better compression compared to KLT and GL-GBST. Also for angular modes (e.g., diagonal mode) in intra predicted coding, GL-GBNT significantly outperforms GL-GBST as expected.

Table V demonstrates the RDOT coding performance of EA-GBTs for different modes by comparing against GL-GBT (corresponding to using GL-GBNT for intra and GL-GBST for inter predicted blocks in $\mathcal{T}_{\text{GL-GBT}} = \{\text{DCT}, \text{GL-GBT}\}$). As shown in the table, the contribution of EA-GBT within the transform set $\mathcal{T}_{\text{GL-GBT+EA-GBT}} = \{\text{DCT}, \text{GL-GBT}, \text{EA-GBT}\}$ is limited to 0.3% for intra predicted coding, while it is approximately 0.8% for inter coding. On the other hand, if the transform set is selected as $\mathcal{T}_{\text{EA-GBT}} = \{\text{DCT}, \text{EA-GBT}\}$ the contribution of EA-GBT provides considerable coding gains, which are approximately 0.5% for intra and 1% for inter predicted coding. Moreover, the percentages of transforms selected using RDOT with the sets $\mathcal{T}_{\text{GL-GBT}}$, $\mathcal{T}_{\text{EA-GBT}}$ and $\mathcal{T}_{\text{GL-GBT+EA-GBT}}$ are presented in Table VI. The most frequently used transforms are GL-GBT and DCT for intra and inter predicted residuals, respectively. Besides, EA-GBT in $\mathcal{T}_{\text{EA-GBT}}$ is used about 10% of the blocks for both intra and inter predicted residuals, and it is less frequently used within the set $\mathcal{T}_{\text{GL-GBT+EA-GBT}}$. Figure 15 further illustrates the transform selection from $\mathcal{T}_{\text{GL-GBT+EA-GBT}}$ in two sample frames of the *BasketballDrill* sequence, where EA-GBT is selected in blocks with sharp discontinuities and GL-GBTs are often selected for blocks with more directional structures as compared to DCT.

VIII. CONCLUSIONS

In this work, we discuss the class of transforms, called graph-based transforms (GBTs), with their applications to video compression. In particular, separable and nonseparable GBTs are introduced and two different design strategies are proposed. Firstly, the GBT design problem is posed as a graph learning problem, where we estimate graphs from data and the resulting graphs are used to define GBTs (GL-GBTs). Secondly, we propose edge-adaptive GBTs (EA-GBTs) which can be adapted on a per-block basis using side-information (image edges in a given block). We also give theoretical justifications for these two strategies and show that well-known transforms such as DCTs and DSTs are special cases of GBTs, and graphs can be used to design generalized (e.g., DCT-like or DST-like) separable transforms. Our experiments demonstrate that GL-GBTs can provide considerable coding gains with respect to standard transform coding schemes using DCT. In comparison with the Karhunen-Loeve transform (KLT), GL-GBTs are more robust and provide better generalization. Although coding gains obtained by including EA-GBTs in addition to GL-GBTs in the RDOT scheme are limited, using EA-GBTs only provides considerable coding gains over DCT.

Future work includes the development of GBTs on state-of-the-art video codecs. Along this line of research, Egilmez *et al.* [45] have recently introduced a practical implementation

of GL-GBTs by replacing the DST-7 and DCT-8 in multiple transform selection (MTS) scheme of VVC [9] with separable GBTs¹⁴. The experiments conducted on the VVC reference software (VTM) show that considerable coding improvements (about 0.4% in BD-rate reduction on average) can be achieved without any impact on encoder and decoder run-times. Thus, the findings in [45] further validate our empirical and theoretical results in this paper and demonstrate the relevance of GBTs in a state-of-the-art codec such as VVC.

REFERENCES

- [1] H. E. Egilmez, A. Said, Y.-H. Chao, and A. Ortega, "Graph-based transforms for inter predicted video coding," in *IEEE International Conference on Image Processing (ICIP)*, Sept 2015, pp. 3992–3996.
- [2] H. E. Egilmez, Y. H. Chao, A. Ortega, B. Lee, and S. Yea, "GBST: Separable transforms based on line graphs for predictive video coding," in *2016 IEEE International Conference on Image Processing (ICIP)*, Sept 2016, pp. 2375–2379.
- [3] H. E. Egilmez, "Graph-based models and transforms for signal/data processing with applications to video coding," Ph.D. dissertation, University of Southern California, 2017.
- [4] Y.-H. Chao, "Compression of signals on graphs with application to image and video coding," Ph.D. dissertation, University of Southern California, 2017.
- [5] W. B. Pennebaker and J. L. Mitchell, *JPEG Still Image Data Compression Standard*, 1st ed. Norwell, MA, USA: Kluwer Academic Publishers, 1992.
- [6] G. J. Sullivan, J.-R. Ohm, W.-J. Han, and T. Wiegand, "Overview of the High Efficiency Video Coding (HEVC) Standard," *IEEE Trans. Circuits Syst. Video Technol.*, vol. 22, no. 12, pp. 1649–1668, Dec. 2012.
- [7] D. Mukherjee, J. Bankoski, R. S. Bultje, A. Grange, J. Han, J. Koleszar, P. Wilkins, and Y. Xu, "The latest open-source video codec VP9 – an overview and preliminary results," in *Proc. 30th Picture Coding Symp.*, San Jose, CA, Dec. 2013.
- [8] Y. Chen, D. Murherjee, J. Han, A. Grange, Y. Xu, Z. Liu, S. Parker, C. Chen, H. Su, U. Joshi, C. Chiang, Y. Wang, P. Wilkins, J. Bankoski, L. Trudeau, N. Egge, J. Valin, T. Davies, S. Midtskogen, A. Norkin, and P. de Rivaz, "An overview of core coding tools in the AV1 video codec," in *2018 Picture Coding Symposium (PCS)*, June 2018, pp. 41–45.
- [9] B. Bross, J. Chen, S. Liu, and Y.-K. Wang, "Versatile video coding (draft 10)," Joint Video Exploration Team (JVET) of ITU-T SG16 WP3 and ISO/IEC JTC 1/SC29/WG11, Output Document JVET-S2001, Jul. 2020.
- [10] J. Han, A. Saxena, V. Melkote, and K. Rose, "Jointly optimized spatial prediction and block transform for video and image coding," *IEEE Trans. Image Process.*, vol. 21, no. 4, pp. 1874–1884, Apr. 2012.
- [11] Y. Ye and M. Karczewicz, "Improved H.264 intra coding based on bi-directional intra prediction, directional transform, and adaptive coefficient scanning," in *IEEE International Conference on Image Processing (ICIP)*, Oct 2008, pp. 2116–2119.
- [12] S. Takamura and A. Shimizu, "On intra coding using mode dependent 2D-KLT," in *Proc. 30th Picture Coding Symp.*, San Jose, CA, Dec. 2013, pp. 137–140.
- [13] A. Arrufat, P. Philippe, and O. Deforges, "Non-separable mode dependent transforms for intra coding in HEVC," in *2014 IEEE Visual Communications and Image Processing Conference*, Dec 2014, pp. 61–64.
- [14] F. Zou, O. Au, C. Pang, J. Dai, X. Zhang, and L. Fang, "Rate-distortion optimized transforms based on the lloyd-type algorithm for intra block coding," *IEEE Journal of Selected Topics in Signal Processing*, vol. 7, no. 6, pp. 1072–1083, Dec 2013.
- [15] X. Zhao, J. Chen, A. Said, V. Seregin, H. E. Egilmez, and M. Karczewicz, "NSST: Non-separable secondary transforms for next generation video coding," in *2016 Picture Coding Symposium (PCS 2016)*, December 2016.
- [16] A. Said, X. Zhao, M. Karczewicz, H. E. Egilmez, V. Seregin, and J. Chen, "Highly efficient non-separable transforms for next generation video coding," in *2016 Picture Coding Symposium (PCS)*, 2016.

¹⁴The work in [45] was submitted and accepted to the IEEE International Conference on Image Processing [63] while the present paper is under review.

TABLE IV

COMPARISON OF KLT, GL-GBST AND GL-GBNT FOR CODING OF DIFFERENT PREDICTION MODES IN TERMS OF BD-RATE WITH RESPECT TO THE DCT. SMALLER (NEGATIVE) BD-RATES MEAN BETTER COMPRESSION.

Transform Set	Intra Prediction					Inter Prediction		
	Planar	DC	Diagonal	Horizontal	All modes	Square	Rectangular	All modes
\mathcal{T}_{KLT}	-5.79	-4.57	-7.68	-6.14	-6.02	-3.47	-2.93	-3.35
$\mathcal{T}_{\text{GL-GBST}}$	-5.45	-4.12	-3.32	-6.45	-4.61	-3.95	-3.25	-3.89
$\mathcal{T}_{\text{GL-GBNT}}$	-6.27	-5.04	-8.74	-6.53	-6.70	-3.84	-3.18	-3.68

TABLE V

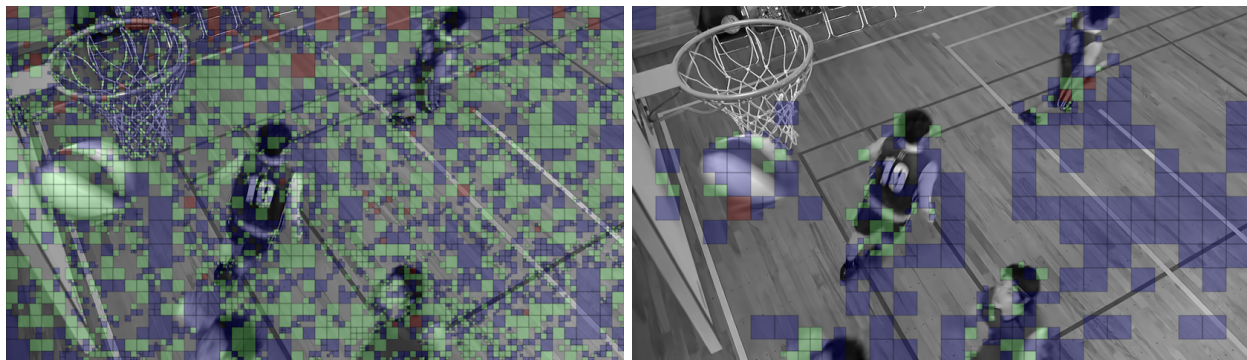
THE CONTRIBUTION OF GL-GBTS AND EA-GBTS IN TERMS OF BD-RATE WITH RESPECT TO THE DCT. GL-GBT CORRESPONDS TO USING GL-GBNT FOR INTRA BLOCKS AND GL-GBST FOR INTER BLOCKS.

Transform Set	Intra Prediction					Inter Prediction		
	Planar	DC	Diagonal	Horizontal	All modes	Square	Rectangular	All modes
$\mathcal{T}_{\text{GL-GBT}}$	-6.27	-5.04	-8.74	-6.53	-6.70	-3.95	-3.25	-3.89
$\mathcal{T}_{\text{EA-GBT}}$	-0.51	-0.47	-0.69	-0.66	-0.54	-1.01	-0.73	-0.93
$\mathcal{T}_{\text{GL-GBT+EA-GBT}}$	-6.58	-5.34	-9.07	-6.89	-7.01	-4.80	-3.65	-4.73

TABLE VI

PERCENTAGE OF TRANSFORMS SELECTED AMONG TRANSFORM CODED BLOCKS BY THE RDOT SCHEME WITH DIFFERENT TRANSFORM SETS. GL-GBT CORRESPONDS TO USING GL-GBNT FOR INTRA BLOCKS AND GL-GBST FOR INTER BLOCKS.

Transform Set	Intra Prediction			Inter Prediction		
	DCT	GL-GBT	EA-GBT	DCT	GL-GBT	EA-GBT
$\mathcal{T}_{\text{GL-GBT}}$	42%	58%	—	73%	27%	—
$\mathcal{T}_{\text{EA-GBT}}$	89%	—	11%	87%	—	13%
$\mathcal{T}_{\text{GL-GBT+EA-GBT}}$	39%	57%	4%	66%	24%	10%



(a) All-intra coded frame (I-frame)

(b) Both intra and inter coded frame (B-frame)

Fig. 15. Illustration of selected transforms from the set $\mathcal{T}_{\text{GL-GBT+EA-GBT}} = \{\text{DCT}, \text{GL-GBT}, \text{EA-GBT}\}$ by the RDOT scheme for each transform coded block. DCT, GL-GBT and EA-GBT are highlighted in purple, green and red, respectively. Most of the blocks in (b) are not transform coded (i.e., transform step is skipped) due to precise inter prediction.

- [17] X. Zhao, J. Chen, M. Karczewicz, A. Said, and V. Seregin, "Joint separable and non-separable transforms for next-generation video coding," *IEEE Transactions on Image Processing*, vol. 27, no. 5, pp. 2514–2525, May 2018.
- [18] T. Biatek, V. Lorcy, and P. Philippe, "Transform competition for temporal prediction in video coding," *IEEE Transactions on Circuits and Systems for Video Technology*, vol. 29, no. 3, pp. 815–826, 2019.
- [19] Y. H. Chao, H. E. Egilmez, A. Ortega, S. Yea, and B. Lee, "Edge adaptive graph-based transforms: Comparison of step/ramp edge models for video compression," in *2016 IEEE International Conference on Image Processing (ICIP)*, Sept 2016, pp. 1539–1543.
- [20] X. Zhao and H. E. Egilmez, "CE6: Summary report on transforms and transform signaling," Joint Video Exploration Team (JVET) of ITU-T SG16 WP3 and ISO/IEC JTC 1/SC29/WG11, Geneva, CH, Input Document JVET-N0026, Mar. 2019.
- [21] X. Zhao, J. Chen, M. Karczewicz, L. Zhang, X. Li, and W. J. Chien, "Enhanced multiple transform for video coding," in *2016 Data Compression Conference (DCC)*, March 2016, pp. 73–82.
- [22] I. M. Johnstone and A. Y. Lu, "On consistency and sparsity for principal components analysis in high dimensions," *Journal of the American Statistical Association*, vol. 104, no. 486, pp. 682–693, 2009.
- [23] P. Ravikumar, M. Wainwright, B. Yu, and G. Raskutti, "High dimensional covariance estimation by minimizing l1-penalized log-determinant divergence," *Electronic Journal of Statistics (EJS)*, vol. 5, pp. 935–980, 2011.
- [24] J. Friedman, T. Hastie, and R. Tibshirani, "Sparse inverse covariance estimation with the graphical lasso," *Biostatistics*, vol. 9, no. 3, pp. 432–441, Jul. 2008.
- [25] H. E. Egilmez, E. Pavez, and A. Ortega, "Graph learning from data under Laplacian and structural constraints," *IEEE Journal of Selected Topics in Signal Processing*, vol. 11, no. 6, pp. 825–841, Sept 2017.
- [26] H. E. Egilmez, E. Pavez, and A. Ortega, "Graph learning from filtered signals: Graph system and diffusion kernel identification," *IEEE Transactions on Signal and Information Processing over Networks*, vol. 5, no. 2, pp. 360–374, June 2019.
- [27] C. Zhang and D. Florencio, "Analyzing the optimality of predictive transform coding using graph-based models," *IEEE Signal Process. Lett.*, vol. 20, no. 1, pp. 106–109, 2013.

- [28] C. Zhang, D. Florencio, and P. Chou, "Graph signal processing - a probabilistic framework," Microsoft Research, Tech. Rep. MSR-TR-2015-31, April 2015. [Online]. Available: <http://research.microsoft.com/apps/pubs/default.aspx?id=243326>
- [29] E. Pavez, H. E. Egilmez, Y. Wang, and A. Ortega, "GTT: Graph template transforms with applications to image coding," in *Picture Coding Symposium (PCS)*, 2015, May 2015, pp. 199–203.
- [30] G. Fracastoro, D. Thanou, and P. Frossard, "Graph transform optimization with application to image compression," *IEEE Transactions on Image Processing*, vol. 29, pp. 419–432, 2020.
- [31] G. Shen, W.-S. Kim, S. Narang, A. Ortega, J. Lee, and H. Wey, "Edge-adaptive transforms for efficient depth map coding," in *Picture Coding Symposium (PCS)*, 2010, Dec 2010, pp. 566–569.
- [32] W. Hu, G. Cheung, A. Ortega, and O. C. Au, "Multiresolution graph fourier transform for compression of piecewise smooth images," *IEEE Transactions on Image Processing*, vol. 24, no. 1, pp. 419–433, Jan 2015.
- [33] F. R. K. Chung, *Spectral Graph Theory*. USA: American Mathematical Society, 1997.
- [34] D. Koller and N. Friedman, *Probabilistic Graphical Models: Principles and Techniques - Adaptive Computation and Machine Learning*. Cambridge, MA, USA: The MIT Press, 2009.
- [35] H. Rue and L. Held, *Gaussian Markov Random Fields: Theory and Applications*, ser. Monographs on Statistics and Applied Probability. London: Chapman & Hall, 2005, vol. 104.
- [36] A. K. Jain, *Fundamentals of Digital Image Processing*. Upper Saddle River, NJ, USA: Prentice-Hall, Inc., 1989.
- [37] A. M. Tekalp, *Digital Video Processing*, 2nd ed. Upper Saddle River, NJ, USA: Prentice Hall Press, 2015.
- [38] M. A. Woodbury, *Inverting Modified Matrices*, ser. Statistical Research Group Memorandum Reports. Princeton, NJ: Princeton University, 1950, no. 42.
- [39] G. Strang, "The discrete cosine transform," *SIAM Rev.*, vol. 41, no. 1, pp. 135–147, Mar. 1999.
- [40] W. Hu, G. Cheung, and A. Ortega, "Intra-prediction and generalized graph Fourier transform for image coding," *IEEE Signal Processing Letters*, vol. 22, no. 11, pp. 1913–1917, Nov 2015.
- [41] M. Püschel and J. M. F. Moura, "Algebraic signal processing theory: 1-D space," *IEEE Transactions on Signal Processing*, vol. 56, no. 8, pp. 3586–3599, 2008.
- [42] H. E. Egilmez, E. Pavez, and A. Ortega, "GLL: Graph Laplacian learning package, version 1.0," https://github.com/STAC-USC/Graph_Learning, 2017.
- [43] H. E. Egilmez, O. G. Guleryuz, J. Ehmann, and S. Yea, "Row-column transforms: Low-complexity approximation of optimal non-separable transforms," in *2016 IEEE International Conference on Image Processing (ICIP)*, Sept 2016, pp. 2385–2389.
- [44] E. Pavez, A. Ortega, and D. Mukherjee, "Learning separable transforms by inverse covariance estimation," in *2017 IEEE International Conference on Image Processing (ICIP)*, 2017, pp. 285–289.
- [45] H. E. Egilmez, O. Teke, A. Said, V. Seregin, and M. Karczewicz, "Parametric graph-based separable transforms for video coding," *CoRR*, vol. abs/arXiv:1911.06981, 2019. [Online]. Available: <https://arxiv.org/abs/1911.06981>
- [46] A. Said, H. E. Egilmez, and Y. H. Chao, "Low-complexity transform adjustments for video coding," in *2019 IEEE International Conference on Image Processing (ICIP)*, Sep. 2019, pp. 1188–1192.
- [47] A. Gersho and R. M. Gray, *Vector Quantization and Signal Compression*. Norwell, MA, USA: Kluwer Academic Publishers, 1991.
- [48] V. K. Goyal, "Theoretical foundations of transform coding," *IEEE Signal Processing Magazine*, vol. 18, no. 5, pp. 9–21, Sep 2001.
- [49] S. Mallat, *A Wavelet Tour of Signal Processing, Third Edition: The Sparse Way*, 3rd ed. Academic Press, 2008.
- [50] V. N. Vapnik, "An overview of statistical learning theory," *IEEE Transactions on Neural Networks*, vol. 10, no. 5, pp. 988–999, Sep 1999.
- [51] U. von Luxburg and B. Schölkopf, *Statistical Learning Theory: Models, Concepts, and Results*. Amsterdam, Netherlands: Elsevier North Holland, May 2011, vol. 10, pp. 651–706.
- [52] R. Vershynin, "How close is the sample covariance matrix to the actual covariance matrix?" *Journal of Theoretical Probability*, vol. 25, no. 3, pp. 655–686, 2012.
- [53] I. Daribo, D. Florencio, and G. Cheung, "Arbitrarily shaped motion prediction for depth video compression using arithmetic edge coding," *IEEE Transactions on Image Processing*, vol. 23, no. 11, pp. 4696–4708, Nov 2014.
- [54] M. Effros, H. Feng, and K. Zeger, "Suboptimality of the Karhunen-Loeve transform for transform coding," *IEEE Transactions on Information Theory*, vol. 50, no. 8, pp. 1605–1619, Aug 2004.
- [55] T. M. Cover and J. A. Thomas, *Elements of Information Theory*. New York, NY, USA: Wiley-Interscience, 1991.
- [56] Xiph.Org Foundation, "Xiph.org video test media." [Online]. Available: <https://media.xiph.org/video/derf/>
- [57] F. Bossen, "JVET common test conditions and software reference configurations for SDR video," Common test conditions and software reference configurations, Geneva, CH, Output Document JCTVC-L1100, Jan. 2013.
- [58] O. Sezer, O. Guleryuz, and Y. Altunbasak, "Approximation and compression with sparse orthonormal transforms," *IEEE Transactions on Image Processing*, vol. 24, no. 8, pp. 2328–2343, Aug 2015.
- [59] WebM Project, "Grand challenge on the use of image restoration for video coding efficiency improvement - ICIP 2017." [Online]. Available: <https://webmproject.github.io/icip-2017/>
- [60] A. Said, "Introduction to Arithmetic Coding: theory and practice," HP Labs, Tech. Rep. HPL-2004-76, 2004.
- [61] A. Ortega and K. Ramchandran, "Rate-distortion methods for image and video compression," *IEEE Signal Process. Mag.*, vol. 15, no. 6, pp. 23–50, Nov. 1998.
- [62] G. Bjontegaard, "Calculation of average PSNR differences between RD-curves," *ITU-T Q.6/SG16 VCEG-M33 Contribution*, vol. 48, Apr 2001.
- [63] H. E. Egilmez, O. Teke, A. Said, V. Seregin, and M. Karczewicz, "Parametric graph-based separable transforms for video coding," in *2020 IEEE International Conference on Image Processing (ICIP)*, Oct. 2020.